BIBECHANA
Vol. 23, No. 1, January 2026, 17-30

ISSN 2091-0762 (Print), 2382-5340 (Online)
Journal homepage: http://nepjol.info/index.php/BIBECHANA
Publisher:Dept. of Phys., Mahendra Morang A. M. Campus (Tribhuvan University)Biratnagar

Quantum chemical characterization and *In Silico* evaluation of Allicin and Trigonelline as EED inhibitors: A DFT, molecular docking, and ADMET study

Bishal Budha[1], Madan Khanal[2], Arjun Acharya[1,*]

[1] *Tri-Chandra Multiple Campus, Tribhuvan University, Kathmandu 44600, Nepal*
[2] *Central Department of Physics, Tribhuvan University, Kathmandu 44600, Nepal*
*Corresponding author. Email: arjun.acharya@trc.tu.edu.np

Abstract

Aberrant regulation of Polycomb Repressive Complex 2 (PRC2), a key epigenetic modulator, is strongly linked to oncogenesis, making it a therapeutic target for epigenetic interventions. Among inhibition strategies, selectively interfering with Embryonic Ectoderm Development (EED), a core PRC2 subunit, has shown greater specificity and efficacy than direct EZH2 inhibition. In this context, two phytochemicals, Allicin and Trigonelline, previously reported for anticancer activities, were investigated for potential interaction with EED. Density Functional Theory (DFT)-based quantum chemical analyses, including HOMO-LUMO energy levels, energy gaps, and global reactivity descriptors, were employed to assess chemical reactivity. Molecular electrostatic potential (MEP) surfaces and Mulliken charge distributions further elucidated electronic behavior and charge localization. Molecular docking simulations revealed that Allicin and Trigonelline bind effectively to EED, with binding affinities of –3.82 and –3.89 kcal/mol, respectively. Taken together, these findings highlight their potential as lead probes for PRC2-targeted therapy, supported by favorable ADMET profiles.

Keywords: Cancer, EED, Phytochemicals, DFT, Protein-Ligand, ADMET. .

Article information
Manuscript received: June 11, 2025; Revised: September 18, 2025; Accepted: September 19, 2025
DOI https://doi.org/10.3126/bibechana.v23i1.80070
This work is licensed under the Creative Commons CC BY-NC License. https://creativecommons.org/licenses/by-nc/4.0/

1 Introduction

Cancer poses a persistent and global medical challenge due to its hallmark features of unchecked cell proliferation and evasion of apoptosis. While genetic alterations are acknowledged as primary contributors to tumorigenesis, accumulating evidence highlights the pivotal influence of epigenetic misregulation, particularly abnormal transcriptional silencing, in promoting oncogenic progression [1]. Among the various epigenetic regulators, the Polycomb Repressive Complex 2 (PRC2) stands out as a central player in tumor biology [2]. This complex functions as a histone methyltransferase that mediates gene silencing through trimethylation of histone H3 at lysine 27 (H3K27me3), an epigenetic modification associated with transcriptional repression [2, 3].

PRC2 consists of core subunits—EZH2 or EZH1 (catalytic), EED, SUZ12, and RBBP4/7—which assemble with accessory factors such as JARID2,

AEBP2, and PCLs to form a functional gene-silencing complex [4]. EZH2 and EZH1, through their SET domains, catalyze the mono-, di-, and trimethylation of H3K27, with trimethylated form (H3K27me3) being crucial for gene repression [5]. Although homologous, EZH2-containing PRC2 complexes display stronger methyltransferase activity and are frequently overexpressed or mutated in malignancies such as lymphomas and carcinomas [6, 7]. Current therapies primarily target EZH2's catalytic activity with S-adenosylmethionine (SAM)-competitive inhibitors, but these agents face challenges including limited efficacy against EZH1, off-target toxicity, and resistance from secondary EZH2 mutations [8–10]. This necessitates alternative therapeutic strategies that bypass direct catalytic inhibition while addressing these limitations.

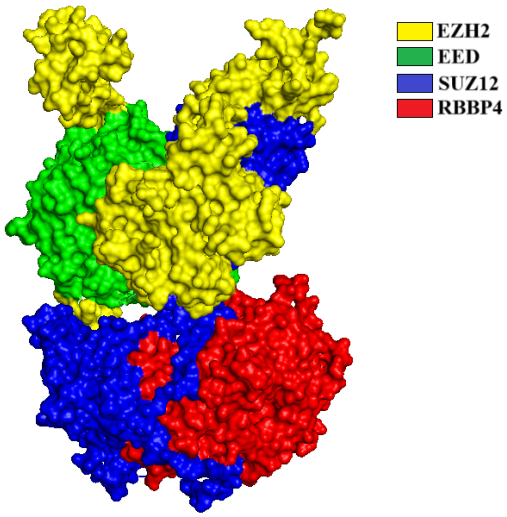

Figure 1: structural conformation image of major subunits of PRC2. (PDB ID: 6c24)

A promising alternative lies in targeting EED, a WD40-repeat subunit of PRC2 that recognizes H3K27me3 via an aromatic cage (H3K27me3 pocket), thereby allosterically activating EZH2 and reinforcing repressive chromatin states [11–13]. Inhibiting this allosteric site disrupts the PRC2 complex's ability to maintain H3K27me3 marks and impairs tumor growth, particularly in cases that are resistant to EZH2 inhibitors [14, 15]. Evidence supporting the therapeutic relevance of the EED pocket underscores its druggability, showing that small-molecule ligands binding to the H3K27me3 recognition site on EED can effectively disrupt the EED–H3K27me3 interaction and attenuate PRC2-mediated methylation activity [16–19]. Recent drug development has focused on EED pocket inhibitors, with several compounds in clinical trials, demonstrating that EED-targeted therapies can destabilize PRC2 and reactivate silenced tumor suppressor genes [17,20], yet none have received FDA approval.

Although these synthetic inhibitors represent a major advancement, challenges such as off-target toxicity, limited bioavailability, and acquired resistance continue to hinder their clinical utility. Consequently, there is increasing interest in phytochemicals as safer, naturally derived epigenetic modulators [21]. Among the various candidates, two small-molecule anticancer compounds—Allicin (predominantly found in *Allium sativum*) and Trigonelline (predominantly found in *Trigonella foenum-graecum*) have exhibited significant anti-tumor activity across both *in vitro* cell-based assays and *in vivo* animal models [22–25]. These effects include anti-proliferative, pro-apoptotic, and anti-metastatic activities across breast, colon, and hematologic cancers [26, 27].

Despite their therapeutic potential, the capacity of these phytochemicals to act as EED-specific inhibitors remains largely unexplored. This research explores the potential of Allicin and Trigonelline to inhibit PRC2 activity by interacting with the H3K27me3 recognition site on EED, proposing an alternative epigenetic intervention. Their structural and electronic characteristics are evaluated through Density Functional Theory (DFT) simulations [28]. Molecular docking is then employed to evaluate binding affinities with the EED protein, focusing on key residues within the aromatic cage, namely Phe97, Tyr148, Trp364, and Tyr365 [29]. Lastly, ADMET analysis determines their pharmacokinetic and toxicity profiles, which are essential for assessing drug-likeness and clinical viability [30, 31].

This integrated computational approach, which includes quantum chemical analysis, molecular docking, and ADMET profiling, aims to validate Allicin and Trigonelline as low-toxicity EED inhibitors. These candidates have the potential to expand the repertoire of PRC2-targeted therapies and enhance treatment outcomes, especially in cases of resistant or refractory cancers.

2 Materials and Methods

2.1 Density Functional Theory (DFT) Calculations

The three-dimensional structures of Allicin (PubChem CID: 65036) and Trigonelline (PubChem CID: 5570) were downloaded from PubChem database. Molecular input files were prepared using GaussView 6 [32] and subsequently optimized using the Gaussian 16W software package [33]. Structural optimizations and electronic property calculations were conducted at the B3LYP/6-311++G(d,p) level of theory, incorporating both ground-state and excited-state computations via

DFT and TD-DFT, respectively [34, 35]. B3LYP has been extensively benchmarked for organic and biological molecules, providing reliable geometries and energetics [36]. The 6-311++G(d,p) basis set includes diffuse and polarization functions essential for modeling polar bonds and hydrogen bonding [37]. This combination was therefore selected for the present study, as it offers a balance between computational cost and accuracy.

Using two key quantum chemical descriptors, HOMO and LUMO, ionization potential (I) and electron affinity (A) were derived on the basis of Koopmans' principles [38], as described in Equations 1 and 2.

$$\text{Ionization potential}(I) = -E_{\text{HOMO}} \quad (1)$$

$$\text{Electron affinity}(A) = -E_{\text{LUMO}} \quad (2)$$

These fundamental descriptors (Eqs. 1 and 2), were further used as basis to evaluate following global reactivity descriptors in equations 3, 4, 5 and 6 [39, 40]:

$$\text{Chemical hardness}(\eta) = \frac{I - A}{2} \quad (3)$$

$$\text{Chemical softness}(S) = \frac{1}{\eta} \quad (4)$$

$$\text{Electronic chemical potential}(\mu) = -\frac{I + A}{2} \quad (5)$$

$$\text{Global electrophilicity index}(\omega) = \frac{\mu^2}{2\eta} \quad (6)$$

Post-optimization visualization and spectral analysis were conducted using GaussView 6, GaussSum 3.0 [41], VEDA4 [42], and Jupyter Notebook [43] for computational scripting and result interpretation.

2.2 Molecular Docking

The high-resolution crystallographic structure of the EED protein complexed with a trimethylated histone H3K27 peptide (PDB ID: 3IIW; resolution: 1.8 Å) was retrieved from the RCSB Protein Data Bank [13]. Structural validation was performed using Ramachandran plot analysis via Discovery Studio Visualizer v21.1.0.20298 [44] to verify backbone geometry accuracy. Subsequent protein preparation involved the removal of non-essential heteroatoms, assignment of polar hydrogen atoms, and the addition of Kollman partial charges. Ligand and receptor structures were processed and converted into PDBQT format using AutoDockTools [45]. Docking simulations were executed using AutoDock 4.2, with a grid box size of 60 × 60 × 60 points, centered at coordinates (x = –15.117, y = –26.084, z = 21.925), and a grid spacing of 0.375 Å. The Lamarckian Genetic Algorithm was applied for the docking protocol, with 2,500,000 energy evaluations, a population size of 300, and up to 27,000 generations per run, executed across 100 runs to ensure exhaustive conformational exploration. The top-ranked protein-ligand complexes, based on binding energy and interaction stability, were analyzed and visualized with the help of PyMOL 2.5.2 [46] and LigPlot+ v2.2 [47] to interpret non-covalent interactions within the binding site.

2.3 Drug-likeness and Toxicity Prediction

ADMET characteristics (Absorption, Distribution, Metabolism, Excretion, and Toxicity) were predicted to investigate the drug-likeness and safety profile of the selected phytochemicals. Canonical SMILES notations for Allicin and Trigonelline were retrieved from the PubChem and submitted to SwissADME [48] for physicochemical, lipophilic, and drug-likeness evaluation. Concurrently, toxicity predictions were conducted using the ProTox-3.0 website [49], allowing estimation of LD50, organ-specific toxicity, and adverse effect pathways.

3 Results and discussion

3.1 DFT calculations

3.1.1 Geometry optimization and stability analysis

Following DFT-based structural optimization, both Allicin and Trigonelline achieved energetically stable conformations, with minimum energy configurations suggesting favorable thermodynamic profiles [50]. The bond parameters of Allicin and Trigonelline, summarized in Tables 1S and 2S, indicate that the longest bonds are S(1)–S(2) in Allicin (2.2358 Å) and C(5)=C(10) in Trigonelline (1.5669 Å), while the shortest are C(8)–H(16) and C(6)–H(12), measuring 1.0838 Å and 1.0811 Å, respectively. The lowest bond angles and dihedral angles occur at S(1)–S(2)–C(5) and C(4)–C(6)–C(8)–H(17) in Allicin, and at N(3)–C(8)–H(14) and C(4)–N(3)–C(6)–C(9) in Trigonelline. The optimized, minimum-energy structures of both compounds in neutral state are illustrated in Figure 2.

Table 1: Calculated energy, dipole moment, and forces in Allicin and Trigonelline.

Compound	Total energy (E) (Hartrees)	Dipole moment (μ) (Debye)	RMS Cartesian force (Hartrees/Bohr)	Maximum Cartesian force (Hartrees/Bohr)
Allicin	–1106.3181	2.7117	6.74×10^{-7}	1.809×10^{-6}
Trigonelline	–476.2606	14.4698	1.474×10^{-6}	8.738×10^{-6}

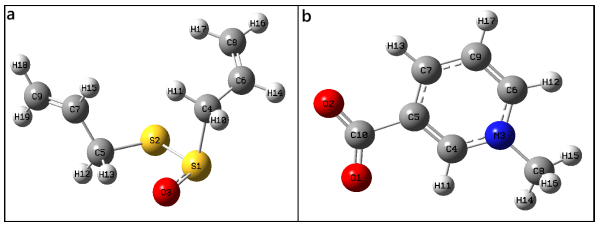

Figure 2: Optimized structures of (a) Allicin and (b) Trigonelline at B3LYP/6-311++G(d,p) level of calculation.

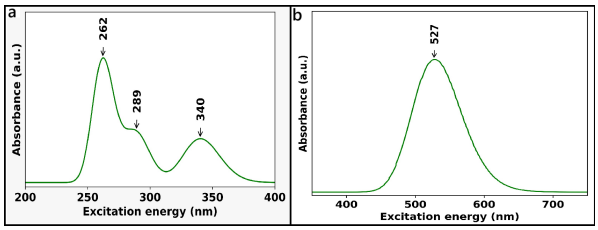

Figure 3: UV-vis spectrum of (a) Allicin and (b)Trigonelline with peak points.

Stability is supported by low RMS and maximum Cartesian force values (Table 1) [51], along with their respective global minimum energies: –1106.3181 Hartrees for Allicin and –476.26062 Hartrees for Trigonelline. These values confirm the conformational integrity of both molecules, which is essential for maintaining structural stability and potential therapeutic function over time [50, 52].

Dipole moment analysis further differentiates the compounds: Allicin exhibits a value of 2.7117 Debye, whereas Trigonelline reaches 14.4698 Debye. The higher polarity of Trigonelline implies stronger intermolecular interactions and enhanced hydrogen bonding potential [53], contributing to better aqueous solubility and possibly improved bioavailability. However, high dipole moments may also limit membrane permeability, underscoring the need to balance polarity based on therapeutic goals [54, 55].

3.1.2 Frontier Molecular Orbitals

For Allicin, electronic transitions are observed at wavelengths of 265.75 nm and 389.6 nm, with the strongest oscillatory transition occurring at 289 nm, corresponding to a HOMO→LUMO excitation, as detailed in Table 2. Trigonelline displays a primary transition at 527.9 nm, with maximum oscillator strength at 528 nm due to a HOMO-2→LUMO transition. In the orbital visualizations, green and red regions denote negative and positive charge phases, respectively [56]. The frontier molecular orbitals (FMOs) provide insights into molecular reactivity and charge distribution [57].

The computed LUMO energies are –1.85 eV for Allicin and –3.05 eV for Trigonelline, indicating higher electron affinity in Allicin. The HOMO–LUMO energy gaps are 4.76 eV for Allicin and 2.76 eV for Trigonelline (Figure 4), consistent with values derived from DOS spectra. A smaller gap in Trigonelline suggests greater electronic softness and reactivity. Compounds with high HOMO energies tend to act as electron donors, whereas low LUMO energies reflect strong electron-accepting abilities [57]. Trigonelline, with a higher HOMO level, functions as a better electron donor than Allicin. The HOMO (E_{H}), LUMO (E_{L}), and their energy gap ($\Delta E_{\mathrm{L\text{-}H}}$) are critical indicators of chemical stability, reactivity, and potential biological activity [58].

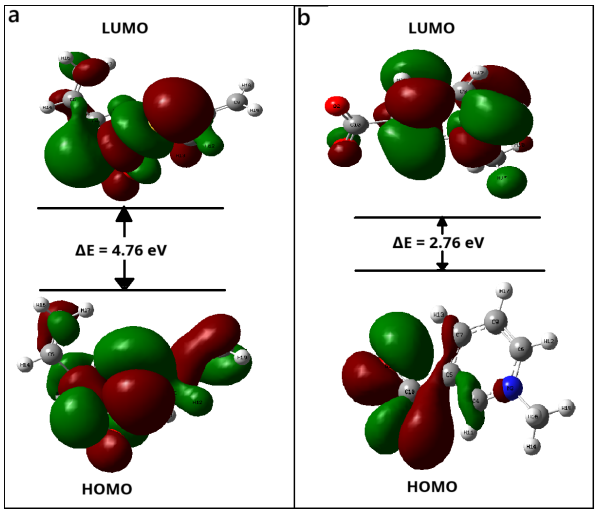

Figure 4: Energy gap between HOMO and LUMO in (a) Allicin and (b)Trigonelline.

The DOS spectrum in Figure 5 illustrates the distribution of electronic states across occupied and

Table 2: Calculated electronic properties of Allicin and Trigonelline.

Compound	Wavelength (nm)	Oscillatory strength	Contributions
Allicin	340	0.0071	HOMO → LUMO (95%)
	289	0.008	HOMO-1 → LUMO (91%) HOMO-4 → LUMO (3%) HOMO-3 → LUMO (2%)
	262	0.02	HOMO → LUMO+1 (87%) HOMO → LUMO+2 (8%)
Trigonelline	642	0.0	HOMO → LUMO (99%)
	637	0.0	HOMO-1 → LUMO (98%)
	528	0.0162	HOMO-2 → LUMO (99%)

virtual orbitals, highlighting electron roles in valence and conduction bands [59]. Collectively, the data suggest that both Allicin and Trigonelline are capable of efficient charge transfer and possess promising biological activity [60].

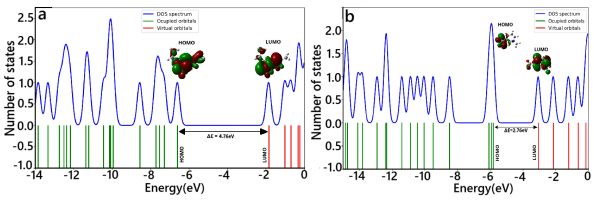

Figure 5: Graphical representation of DOS of (a) Allicin and (b)Trigonelline.

3.1.3 Global Reactivity Descriptors

The computed global electrophilicity index values, 3.76 eV for Allicin and 7.11 eV for Trigonelline, alongside their respective electronic chemical potentials, highlight pronounced electrophilic behavior in both compounds [61]. These values are consistent with charge-exchange tendencies that may enhance their binding affinity in ligand-receptor interactions [61, 62]. The frontier orbitals, HOMO and LUMO, are directly linked to a molecule's ionization potential and electron affinity, respectively, thereby reflecting its electron-donating and accepting capabilities [63]. Molecules with lower ionization potential are more prone to donate electrons, making them efficient radical scavengers [59]. Based on this criterion, Trigonelline, with a lower ionization potential, exhibits comparatively stronger antioxidant potential than Allicin [64]. Additionally, the electronic chemical potential (μ) values of –4.23 eV for Allicin and –4.43 eV for Trigonelline further aid their propensity for electron donation [61]. These electronic properties collectively provide insight into the chemical reactivity and potential biological efficacy of the two phytocompounds.

3.1.4 Molecular Electrostatic Potential (MEP)

MEP map illustrates the distribution of the electrostatic potential across a molecule's surface, thereby identifying reactive regions. Color coding in the MEP map visually distinguishes electrostatic intensity: red represents regions of highest negative potential (strong attraction), followed by yellow and green for intermediate or near-neutral zones, and blue for regions of highest positive potential (strong repulsion). The MEP contour maps for Allicin and Trigonelline are presented in Figure 6.

For Allicin, the electrostatic potential ranges from –0.88 to 0.88 a.u., while for Trigonelline it spans from –0.16 to 0.16 a.u. The oxygen atom O3 in Allicin displays the highest negative potential, denoting a strong nucleophilic site, whereas O1 and O2 serve similar roles in Trigonelline. Regions of maximum positive potential are localized around hydrogen atoms H10, H14, and H17 in Allicin, and H12, H15, H16, and H17 in Trigonelline, suggesting possible sites for electrophilic interactions.

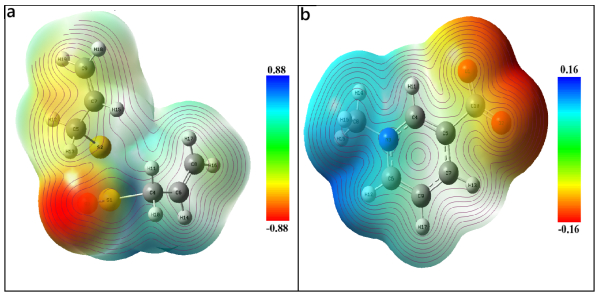

Figure 6: MEP maps together with contour lines for (a) Allicin and (b) Trigonelline.

Of particular interest, both sulfur atoms in Allicin exhibit strongly negative potential regions, which may contribute to its bioactivity [54]. Carbon atoms across both molecules display a mixed electrostatic profile, with surrounding areas showing both positive and negative potentials, corroborating spatial complexity in electron density distribution. This detailed electrostatic mapping aids in

Table 3: Global reactivity descriptors for Allicin and Trigonelline.

Parameter	Allicin	Trigonelline
HOMO	-6.61 eV	-5.81 eV
LUMO	-1.85 eV	-3.05 eV
$E_{\mathbf{LUMO}} - E_{\mathbf{HOMO}}$	4.76 eV	2.76 eV
Ionization Potential Energy (I)	6.61 eV	5.81 eV
Electron Affinity (A)	1.85 eV	3.05 eV
Electronegativity (χ)	4.23 eV	4.43 eV
Electronic Chemical Potential (μ)	-4.23 eV	-4.43 eV
Chemical Hardness (η)	2.38 eV	1.38 eV
Chemical Softness (S)	0.42 $(\text{eV})^{-1}$	0.72 $(\text{eV})^{-1}$
Global Electrophilicity Index (ω)	3.76 eV	7.11 eV

predicting potential sites for electrophilic attacks, nucleophilic attacks, hydrogen bonding, and other intermolecular interactions, which are critical to understanding molecular reactivity and biological behavior [65, 66].

3.1.5 Mulliken Atomic Charges

For Allicin, Mulliken atomic charge analysis (Table 3S) indicates that oxygen atoms carry negative charges, hydrogen atoms are positively charged, and sulfur and carbon atoms exhibit both positive and negative charge distributions, as visualized in Figure 7. In the case of Trigonelline (Table 3S), oxygen atoms similarly show negative charges, while nitrogen and hydrogen atoms are positively charged, with carbon atoms again demonstrating mixed charge states.

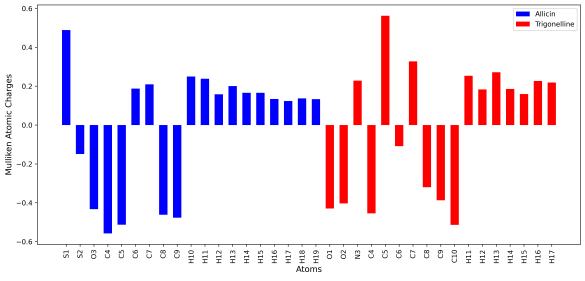

Figure 7: Mulliken atomic charge distributions of Allicin and Trigonelline.

The atom with the highest positive Mulliken charge plays a critical role in molecular interactions [67]. For Allicin, this is observed on the sulfur atom S1, whereas for Trigonelline, it is found on the carbon atom C5. Conversely, the atoms with the most negative charge values are C4 in Allicin and C10 in Trigonelline. Among hydrogen atoms, the most positive charges are located on H10 in Allicin and H13 in Trigonelline.

Mulliken population analysis provides an estimate of partial atomic charges, offering insight into the distribution of electron density within a molecule. This is crucial for understanding how molecules participate in electrophilic and nucleophilic reactions [65]. The observed charge distributions highlight the polar nature of both Allicin and Trigonelline, corroborating their potential for chemical reactivity and biological interaction through charge-mediated binding [66].

3.2 Molecular Docking

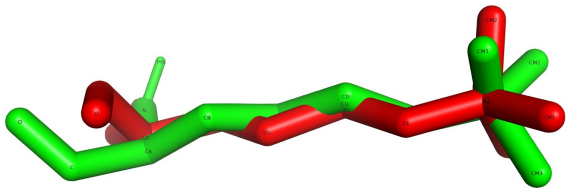

Figure 8: The most matched conformations during re-docking.

Initially, the native co-crystallized ligand of EED was subjected to re-docking into its original binding pocket, to validate the reliability of the docking approach. The structural deviation between the experimentally determined and re-docked conformations was quantified by finding the Root Mean Square Deviation (RMSD) using the DockRMSD utility, thereby validating the accuracy and reproducibility of the docking protocol. The optimal alignment was achieved after 98 runs, yielding an RMSD of 1.233 Å and a MatchAlign score of 5.000. Visual inspection of the alignment, with the native ligand depicted in red and the re-docked ligand in green, demonstrated high spatial concordance, confirming docking reliability (Figure 8). As the RMSD falls within the acceptable range for docking validation [68], the methodology was deemed suitable for further analysis.

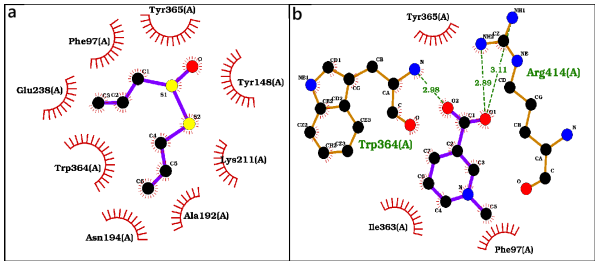

Figure 9: Two-dimensional diagrams of molecular interactions between EED and (a) Allicin and (b) Trigonelline.

Molecular docking analysis revealed that Allicin interacts with the EED protein primarily through hydrophobic contacts involving Phe97, Tyr365, Tyr148, Lys211, Ala192, Asn194, Trp364, and Glu238 (Figure 9 & Table 4). The calculated binding energy of Allicin at the H3K27me3 recognition site (H3K27me3 pocket) was –3.82 kcal/mol, with an associated inhibition constant of 1.59 mM. Trigonelline formed hydrophobic interactions with Tyr365, Ile363, and Phe97, and established three hydrogen bonds: one with Trp364 at 2.98 Å, and two with Arg414 at 2.89 Å and 3.11 Å. The total binding energy was slightly lower than that of Allicin at –3.89 kcal/mol, with an inhibition constant of 1.42 mM (Table 5). The additional hydrogen bonding observed in the Trigonelline–EED complex likely contributes to its enhanced binding affinity relative to Allicin, in agreement with predictions made earlier based on dipole moment values.

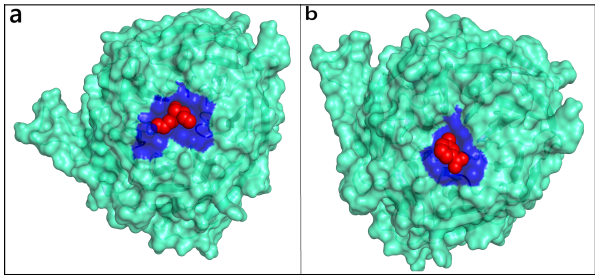

Figure 10: 3D Conformations of the EED-Allicin and EED-Trigonelline complexes.

Both compounds exhibit negative binding energies with EED, indicating favorable interactions and reinforcing their potential as EED inhibitors. The predicted 3D binding conformations for EED–Allicin and EED–Trigonelline are shown in Figure 10, while the corresponding 2D interaction diagrams highlighting the participating residues are provided in Figure 11.

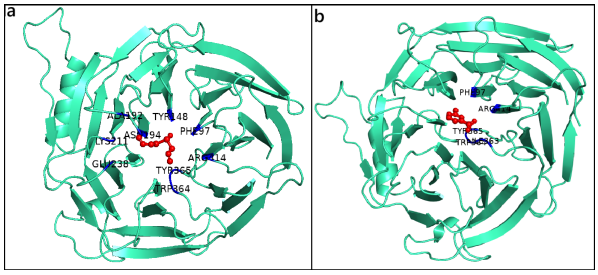

Figure 11: PyMOL-rendered 2D conformational images of EED-Allicin and EED-Trigonelline complexes.

It is worth noting that DFT-based MEP and Mulliken charge analyses previously identified O1 and O2 in Trigonelline as the most electronegative sites. These atoms were confirmed to engage in hydrogen bonding during docking, validating the predictive accuracy of the quantum chemical descriptors. Most atoms anticipated to participate in interactions, based on electronic and electrostatic mapping, were indeed involved in binding.

3.3 Ramachandran Plot

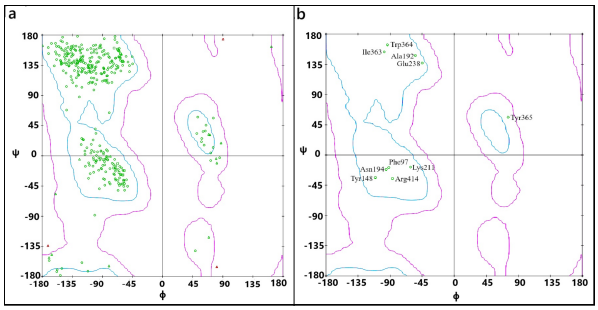

Figure 12: Ramachandran plots for (a) all residues of EED and (b) residues interacting with selected phytochemicals.

All EED residues involved in interactions with Allicin and Trigonelline, namely Tyr365, Trp364, Ala192, Glu238, Tyr148, Arg414, Ile363, Lys211, Phe97, and Asn194, are located within the permitted zone of the Ramachandran plot (Figure 12). This structural validation confirms the reliability of the protein-ligand interactions [69]. Additionally, the majority of the residues in the EED structure fall within the allowed regions, thereby confirming the conformational integrity of the targeted receptor. The Ramachandran plot is used to visualize the torsional angles phi (ϕ) on the x-axis and psi (ψ) on the y-axis, serving as a critical reference for validating protein geometry. Figure 12 and Table 4S provide a detailed overview of these torsional angles for both the entire EED structure and its active-site residues.

Table 4: Interactions of EED protein residues with Allicin and Trigonelline.

Ligand	Binding residues	Atoms	Bond length (Å)	Interactions
Allicin	Phe97, Tyr365, Tyr148 Lys211, Ala192, Asn194 Trp364, Glu238	-	-	Non-bonded
Trigonelline	TRP364	N-O2	2.98	H-bonds
	ARG414	NH2-O1	2.89	H-bonds
	ARG414	NH1-O1	3.11	H-bonds
	TYR365, PHE97, ILE363	-	-	Non-bonded

Table 5: Molecular docking results for EED-Allicin and EED-Trigonelline complexes.

Parameters	EED-Allicin complex	EED-Trigonelline complex
Final Intermolecular Energy (kcal/mol)	-5.31	-4.18
Final Total Internal Energy (kcal/mol)	-0.28	0.09
Torsional Free Energy (kcal/mol)	1.49	0.30
Unbound System's Energy (kcal/mol)	-0.28	0.09
Estimated Free Energy of Binding (kcal/mol)	-3.82	-3.89
Inhibition Constant (mM)	1.59	1.42

3.4 Drug-Likeness and Toxicity

The lipophilicity of Allicin and Trigonelline, as indicated by their consensus Log P values (Table 6), was found to be below 5, within acceptable threshold for drug-like properties [48]. The Log S (ESOL) values of –1.34 (Allicin) and –1.39 (Trigonelline) indicate good aqueous solubility and imply promising metabolic potential in biological systems [70]. These results are consistent with the solubility classification by Sorkun et al., where Log S values near 0 indicate solubility, while more negative values (< -4) are typically associated with poor solubility. Further solubility indicators such as Log S (Ali) and Log S (SILICOS-IT) revealed values of –2.20 and –1.70 for Allicin, and –1.00 and –0.94 for Trigonelline, respectively. These findings suggest moderate to high solubility. Balanced lipophilicity is essential for effective absorption and membrane permeability [71], and both compounds appear well-positioned in this regard, as detailed in Table 6.

According to Lipinski's Rule of Five [72], both compounds meet the criteria for oral bioavailability: molecular weight below 500 Da, no more than five hydrogen bond donors, no more than ten hydrogen bond acceptors, and Log P below 5 (Table 7). Both also complied with the Veber and Egan rules but failed to meet all criteria set by Ghose and Muegge filters.

Pharmacokinetic profiling (Table 8) indicated high gastrointestinal absorption for both compounds, with limited permeability through P-glycoprotein (PGP), moderate skin penetration, and acceptable Log Kp values. Allicin was predicted to cross the blood-brain barrier (BBB), whereas Trigonelline was not. BBB permeability may result in unintended central nervous system (CNS) exposure [73], raising concerns about potential neurological toxicity of Allicin. This observation warrants further investigation into its off-target CNS effects. Neither compound inhibited major cytochrome P450 isoenzymes (CYP1A2, CYP2D6, CYP2C19, CYP2C9, and CYP3A4), underscoring minimal risk of drug–drug interactions affecting hepatic metabolism [74].

Table 6: Predictive physicochemical properties of Allicin and Trigonelline.

Properties	Allicin	Trigonelline
Molecular weight (g/mol)	162.27	137.14
Number of heavy atoms	9	27
Lipophilicity:		
Log $P_{o/w}$ (ILOGP)	1.95	-3.11
Log $P_{o/w}$ (XLOGP3)	1.31	0.51
Log $P_{o/w}$ (WLOGP)	2.62	-1.13
Log $P_{o/w}$ (MLOGP)	1.18	0.33
Log $P_{o/w}$ (SILICOS-IT)	0.96	0.36
Consensus Log $P_{o/w}$	1.61	-0.61
Water Solubility:		
Log S (ESOL)	-1.34	-1.39
Log S (Ali)	-2.20	-1.00
Log S (SILICOS-IT)	-1.70	-0.94

The drug-likeness radar plot (Figure 13) based on parameters such as lipophilicity, size, solubility, polarity, flexibility, and saturation indicated that Allicin fits well within the ideal physicochemical space (pink region) [48]. Trigonelline showed a slight deviation in the saturation parameter but retained overall advantageous characteristics for drug candidacy.

Table 7: Predictive Drug-likeness of Allicin and Trigonelline.

Compound	Lipinski	Ghose	Veber	Egan	Muegge	Bioavailability Score
Allicin	Yes	No	Yes	Yes	No	0.55
Trigonelline	Yes	No	Yes	Yes	No	0.55

Table 8: Predicted pharmacokinetic properties of Allicin and Trigonelline.

Properties	Allicin	Trigonelline
GIA absorption	High	High
BBB permeation	Yes	No
CYP1A2 inhibitor	No	No
CYP2B6 inhibitor	No	No
CYP2C19 inhibitor	No	No
CYP2D6 inhibitor	No	No
CYP3A4 inhibitor	No	No
Log K_p (cm/s)	-6.36	-6.77

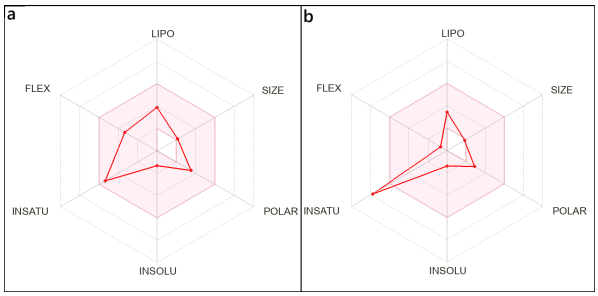

Figure 13: Bioavailability radar plot of (a) Allicin and (b) Trigonelline

In the BOILED-Egg model (Figure 14), Trigonelline appears in the white region, indicating high gastrointestinal absorption and active efflux by PGP (PGP^+), whereas Allicin lies within the yellow zone, suggesting BBB permeability and PGP-mediated efflux [48].

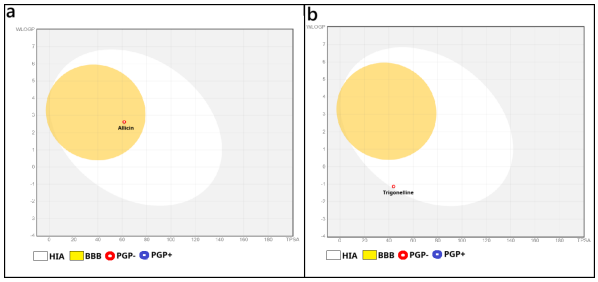

Figure 14: BOILED-Egg image representation of (a) Allicin and (b) Trigonelline.

Toxicological predictions based on LD_{50} values (mg/kg body weight) categorized Allicin (874 mg/kg) as moderately toxic and Trigonelline (3720 mg/kg) as having low toxicity [75]. According to the Globally Harmonized System (GHS), Allicin and Trigonelline fall into categories 4 and 5, respectively, reflecting moderate and minimal acute toxicity [75]. Trigonelline was predicted to induce respiratory and neurotoxic effects, while Allicin exhibited no organ-specific toxicity (Table 9).

Table 9: Toxicity prediction outcomes of Allicin and Trigonelline.

Properties	Allicin	Trigonelline
LD50 (mg/kg)	874	3720
Predicted Toxicity Class	4	5
Organ Toxicity:		
Hepatotoxicity	Inactive	Inactive
Neurotoxicity	Inactive	Active
Nephrotoxicity	Inactive	Inactive
Respiratory Toxicity	Inactive	Active
Cardiotoxicity	Inactive	Inactive
Toxicity end points:		
Carcinogenicity	Inactive	Inactive
Immunotoxicity	Inactive	Inactive
Mutagenicity	Inactive	Inactive
Cytotoxicity	Inactive	Inactive
BBB-barrier	Active	Active
Ecotoxicity	Inactive	Active
Clinical toxicity	Inactive	Inactive
Nutritional toxicity	Inactive	Inactive

Furthermore, toxicity endpoint screening indicated that both compounds may cross the BBB but do not interact with key toxicological pathways, including the aryl hydrocarbon receptor, aromatase, nuclear factor (erythroid-derived 2), estrogen receptor, heat shock factor response element, or mitochondrial membrane potential. These observations collectively substantiate their low systemic toxicity and potential therapeutic viability.

4 Conclusion

The present investigation delivers a thorough analysis of the quantum chemical and pharmacological properties of two phytochemicals, Allicin and Trigonelline, through Density Functional Theory (DFT) and ADMET profiling. Furthermore, molecular docking analysis was employed to explore how these compounds interact with the EED subunit of the Polycomb Repressive Complex 2 (PRC2), to evaluate their potential as epigenetic modulators in cancer treatment. Quantum chemical descriptors, including HOMO–LUMO energy gaps,

dipole moments, and global reactivity indices, revealed that both molecules possess favorable electronic characteristics that underpin their reactivity and biological relevance. Their binding affinities to EED were –3.89 kcal/mol for Trigonelline and –3.82 kcal/mol for Allicin, indicating stable and energetically favorable interactions, facilitated through hydrogen bonding and hydrophobic contacts. In addition, ADMET profiling demonstrated their drug-likeness, with both compounds displaying acceptable lipophilicity, solubility, and high gastrointestinal absorption. Trigonelline exhibited superior aqueous solubility, whereas Allicin showed better performance in radar plot analysis, falling within the optimal physicochemical space for oral drug candidates. The toxicity risk assessment, based on LD_{50} values, classified both compounds with low to moderate toxicity, supporting their suitability for therapeutic consideration. Collectively, the findings suggest that Allicin and Trigonelline meet key criteria for potential EED inhibition, exhibiting favorable electronic, pharmacokinetic, and safety profiles. While the findings lay a promising groundwork, comprehensive assessments using laboratory-based and live model experiments are crucial to confirm both their therapeutic effectiveness and biological safety in epigenetic applications.

Acknowledgment

We acknowledge and appreciate Prof. Dr. Rajendra Parajuli and Asst. Prof. Pitamber Shrestha from Amrit Campus, T.U., for providing access to the Gaussian 16W software. Our deep respect and gratitude to Prof. Dr. Hari Lamichhane from the CDP, T.U., for facilitating the computational resources and providing valuable suggestions. Furthermore, we are grateful to Mr. Shishir Paudel for his support in generating the graphs and figures and for his valuable suggestions. With the aggregative efforts and help from these individuals have made this project possible.

Author Contributions

Bishal Budha: Conceptualization, Methodology, Investigation, Visualization, Data curation, Formal analysis, Validation, Writing – original draft. **Madan Khanal:** Validation, Formal analysis, Software, Supervision, Writing – review & editing. **Arjun Acharya:** Project administration, Formal analysis, Resources, Software, Validation, Supervision, Writing – review & editing.

Data Availability

This paper presents most of the data while additional data and analyses are provided in Supplementary Information. The data that are used to create figures and tables are available upon request to the corresponding author.

Declarations and Conflict of Interest

The authors declare that there are no conflicts of interest.

References

[1] Ran Duan, Wenfang Du, and Weijian Guo. EZH2: a novel target for cancer treatment. *Journal of hematology & oncology*, 13(1):104, 2020.

[2] Diego Pasini and Luciano Di Croce. Emerging roles for polycomb proteins in cancer. *Current opinion in genetics & development*, 36:50–58, 2016.

[3] Raphael Margueron, Guohong Li, Kavitha Sarma, Alexandre Blais, Jiri Zavadil, Christopher L Woodcock, Brian D Dynlacht, and Danny Reinberg. EZH1 and EZH2 maintain repressive chromatin through different mechanisms. *Molecular cell*, 32(4):503–518, 2008.

[4] Ying Huang, Martin Sendzik, Jeff Zhang, Zhenting Gao, Yongfeng Sun, Long Wang, Justin Gu, Kehao Zhao, Zhengtian Yu, Lijun Zhang, et al. Discovery of the clinical candidate mak683: an EED-directed, allosteric, and selective PRC2 inhibitor for the treatment of advanced malignancies. *Journal of medicinal chemistry*, 65(7):5317–5333, 2022.

[5] Xiaohua Shen, Yingchun Liu, Yu-Jung Hsu, Yuko Fujiwara, Jonghwan Kim, Xiaohong Mao, Guo-Cheng Yuan, and Stuart H Orkin. EZH1 mediates methylation on histone h3 lysine 27 and complements EZH2 in maintaining stem cell identity and executing pluripotency. *Molecular cell*, 32(4):491–502, 2008.

[6] Ryan D Morin, Nathalie A Johnson, Tesa M Severson, Andrew J Mungall, Jianghong An, Rodrigo Goya, Jessica E Paul, Merrill Boyle, Bruce W Woolcock, Florian Kuchenbauer, et al. Somatic mutations altering EZH2 (tyr641) in follicular and diffuse large b-cell lymphomas of germinal-center origin. *Nature genetics*, 42(2):181–185, 2010.

[7] Damian B Yap, Justin Chu, Tobias Berg, Matthieu Schapira, S-W Grace Cheng, Annie Moradian, Ryan D Morin, Andrew J Mungall, Barbara Meissner, Merrill Boyle, et al. Somatic mutations at EZH2 y641 act dominantly through a mechanism of selectively altered

PRC2 catalytic activity, to increase h3k27 trimethylation. *Blood, The Journal of the American Society of Hematology*, 117(8):2451–2459, 2011.

[8] Liping Chu, Dongxia Tan, Meimei Zhu, Yuxiu Qu, Xin Ma, Bao-Liang Song, and Wei Qi. EZH2 w113c is a gain-of-function mutation in b-cell lymphoma enabling both PRC2 methyltransferase activation and tazemetostat resistance. *Journal of Biological Chemistry*, 299(4), 2023.

[9] Tobias Neff, Amit U Sinha, Michael J Kluk, Nan Zhu, Mohamed H Khattab, Lauren Stein, Huafeng Xie, Stuart H Orkin, and Scott A Armstrong. Polycomb repressive complex 2 is required for mll-af9 leukemia. *Proceedings of the National Academy of Sciences*, 109(13):5028–5033, 2012.

[10] Alexei Brooun, Ketan S Gajiwala, Ya-Li Deng, Wei Liu, Ben Bolaños, Patrick Bingham, You-Ai He, Wade Diehl, Nicole Grable, Pei-Pei Kung, et al. Polycomb repressive complex 2 structure with inhibitor reveals a mechanism of activation and drug resistance. *Nature communications*, 7(1):11384, 2016.

[11] Serena Sanulli, Neil Justin, Aurélie Teissandier, Katia Ancelin, Manuela Portoso, Matthieu Caron, Audrey Michaud, Berangère Lombard, Simao T da Rocha, John Offer, et al. Jarid2 methylation via the PRC2 complex regulates H3K27me3 deposition during cell differentiation. *Molecular cell*, 57(5):769–783, 2015.

[12] Diego Pasini, Paul AC Cloos, Julian Walfridsson, Linda Olsson, John-Paul Bukowski, Jens V Johansen, Mads Bak, Niels Tommerup, Juri Rappsilber, and Kristian Helin. Jarid2 regulates binding of the polycomb repressive complex 2 to target genes in es cells. *Nature*, 464(7286):306–310, 2010.

[13] Raphael Margueron, Neil Justin, Katsuhito Ohno, Miriam L Sharpe, Jinsook Son, William J Drury Iii, Philipp Voigt, Stephen R Martin, William R Taylor, Valeria De Marco, et al. Role of the polycomb protein EED in the propagation of repressive histone marks. *Nature*, 461(7265):762–767, 2009.

[14] Simon Poepsel, Vignesh Kasinath, and Eva Nogales. Cryo-em structures of PRC2 simultaneously engaged with two functionally distinct nucleosomes. *Nature structural & molecular biology*, 25(2):154–162, 2018.

[15] Michael L Curtin, Marina A Pliushchev, Huan-Qiu Li, Maricel Torrent, Justin D Dietrich, Clarissa G Jakob, Haizhong Zhu, Hongyu Zhao, Ying Wang, Zhiqin Ji, et al. Sar of amino pyrrolidines as potent and novel protein-protein interaction inhibitors of the prc2 complex through eed binding. *Bioorganic & Medicinal Chemistry Letters*, 27(7):1576–1583, 2017.

[16] Andreas Lingel, Martin Sendzik, Ying Huang, Michael D Shultz, John Cantwell, Michael P Dillon, Xingnian Fu, John Fuller, Tobias Gabriel, Justin Gu, et al. Structure-guided design of EED binders allosterically inhibiting the epigenetic polycomb repressive complex 2 (PRC2) methyltransferase. *Journal of Medicinal Chemistry*, 60(1):415–427, 2017.

[17] Yupeng He, Sujatha Selvaraju, Michael L Curtin, Clarissa G Jakob, Haizhong Zhu, Kenneth M Comess, Bailin Shaw, Juliana The, Evelyne Lima-Fernandes, Magdalena M Szewczyk, et al. The EED protein–protein interaction inhibitor a-395 inactivates the PRC2 complex. *Nature chemical biology*, 13(4):389–395, 2017.

[18] Ling Li, Hailong Zhang, Man Zhang, Mengxi Zhao, Lijian Feng, Xiao Luo, Zhenting Gao, Ying Huang, Ophelia Ardayfio, Ji-Hu Zhang, et al. Discovery and molecular basis of a diverse set of polycomb repressive complex 2 inhibitors recognition by EED. *PLoS One*, 12(1):e0169855, 2017.

[19] Dading Huang, Shuaizhen Tian, Yifei Qi, and John ZH Zhang. Binding modes of small-molecule inhibitors to the EED pocket of PRC2. *ChemPhysChem*, 21(3):263–271, 2020.

[20] Qichao Bao, Anil Kumar, Daqing Wu, and Jia Zhou. Targeting EED as a key PRC2 complex mediator toward novel epigenetic therapeutics. *Drug Discovery Today*, page 103986, 2024.

[21] A. Scirè, G. Casari, B. Romaldi, C. Minnelli, and D. Marzioni. Epigenetic properties of compounds contained in functional foods against cancer. *Biomolecules*, 15(1):15, 2024. doi: 10.3390/biom15010015.

[22] Katarzyna Kostelecka, Łukasz Bryliński, Olga Komar, Justyna Michalczyk, Agata Miłosz, Jan Biłogras, Filip Woliński, Alicja Forma, and Jacek Baj. An overview of the spices used for the prevention and potential treatment of gastric cancer. *Cancers*, 16(8):1611, 2024.

[23] Nishat Fatima, Syed Shabihe Raza Baqri, Ahmad Alsulimani, Sharmila Fagoonee, Petr Slama, Kavindra Kumar Kesari, Shubhadeep Roychoudhury, and Shafiul Haque. Phytochemicals from indian ethnomedicines:

Promising prospects for the management of oxidative stress and cancer. *Antioxidants*, 10(10):1606, 2021.

[24] Sukhdev Singh, Bhupender Sharma, Shamsher S Kanwar, and Ashok Kumar. Lead phytochemicals for anticancer drug development. *Frontiers in plant science*, 7:1667, 2016.

[25] Nobuhiro Hirakawa, Rieko Okauchi, Yutaka Miura, and Kazumi Yagasaki. Anti-invasive activity of niacin and trigonelline against cancer cells. *Bioscience, biotechnology, and biochemistry*, 69(3):653–658, 2005.

[26] Bahare Salehi, Paolo Zucca, Ilkay Erdogan Orhan, Elena Azzini, Charles Oluwaseun Adetunji, Soheb Anwar Mohammed, Sanjay K Banerjee, Farukh Sharopov, Daniela Rigano, Javad Sharifi-Rad, et al. Allicin and health: A comprehensive review. *Trends in Food Science & Technology*, 86:502–516, 2019.

[27] Vi Nguyen, Elaine G Taine, Dehao Meng, Taixing Cui, and Wenbin Tan. Pharmacological activities, therapeutic effects, and mechanistic actions of trigonelline. *International Journal of Molecular Sciences*, 25(6):3385, 2024.

[28] Kalpana Gyawali, Rajesh Maharjan, Arjun Acharya, Madan Khanal, Madhav Prasad Ghimire, and Tika Ram Lamichhane. Identification of catechin as main protease inhibitor of sars-cov-2 omicron variant using molecular docking, molecular dynamics, pca, dccm, mm/gbsa and admet profiling. *Natural Product Research*, pages 1–8, 2024.

[29] Chao Xu, Chuanbing Bian, Wei Yang, Marek Galka, Hui Ouyang, Chen Chen, Wei Qiu, Huadong Liu, Amanda E Jones, Farrell MacKenzie, et al. Binding of different histone marks differentially regulates the activity and specificity of polycomb repressive complex 2 (PRC2). *Proceedings of the National Academy of Sciences*, 107(45):19266–19271, 2010.

[30] Mamaru Bitew, Tegene Desalegn, Taye B Demissie, Anteneh Belayneh, Milkyas Endale, and Rajalakshmanan Eswaramoorthy. Pharmacokinetics and drug-likeness of antidiabetic flavonoids: Molecular docking and dft study. *Plos one*, 16(12):e0260853, 2021.

[31] Arjun Acharya, Madan Khanal, Rajesh Maharjan, Kalpana Gyawali, Bhoj Raj Luitel, Rameshwar Adhikari, Deependra Das Mulmi, Tika Ram Lamichhane, and Hari Prasad Lamichhane. Quantum chemical calculations on calcium oxalate and dolichin a and their binding efficacy to lactoferrin: An in silico study using dft, molecular docking, and molecular dynamics simulations. *AIMS Biophysics*, 11(2):142–165, 2024.

[32] Roy Dennington, Todd A. Keith, and John M. Millam. Gaussview, version 6, 2016. Semichem Inc., Shawnee Mission, KS.

[33] M Prabhaharan, AR Prabakaran, S Gunasekaran, and S Srinivasan. Molecular structure and vibrational spectroscopic investigation of melamine using dft theory calculations. *Spectrochimica Acta Part A: Molecular and Biomolecular Spectroscopy*, 123:392–401, 2014.

[34] P Jeffrey Hay and Willard R Wadt. Ab initio effective core potentials for molecular calculations. potentials for the transition metal atoms sc to hg. *The Journal of chemical physics*, 82(1):270–283, 1985.

[35] Hari Prasad Lamichhane and Gary Hastings. Calculated vibrational properties of pigments in protein binding sites. *Proceedings of the National Academy of Sciences*, 108(26):10526–10531, 2011.

[36] Ken-ichi Yamada and Tsubasa Inokuma. Evaluation of quantum chemistry calculation methods for conformational analysis of organic molecules using a-value estimation as a benchmark test. *RSC advances*, 13(51):35904–35910, 2023.

[37] Xiao-li Gong, Zheng-yu Zhou, Han Zhang, and Shu-zhen Liu. Density functional theory study of the hydrogen bonding interaction of the dimers of formylhalide. *Journal of Molecular Structure: THEOCHEM*, 718(1-3):23–29, 2005.

[38] Ralph G Pearson. Absolute electronegativity and hardness: application to inorganic chemistry. *Inorganic chemistry*, 27(4):734–740, 1988.

[39] J Padmanabhan, R Parthasarathi, V Subramanian, and PK Chattaraj. Electrophilicity-based charge transfer descriptor. *The Journal of Physical Chemistry A*, 111(7):1358–1361, 2007.

[40] Rajesh Maharjan, Kalpana Gyawali, Arjun Acharya, Madan Khanal, Madhav Prasad Ghimire, and Tika Ram Lamichhane. Artemisinin derivatives as potential drug candidates against mycobacterium tuberculosis: insights from molecular docking, md simulations, pca, mm/gbsa and admet analysis. *Molecular Simulation*, 50(11):717–728, 2024.

[41] N. M. O'Boyle, A. L. Tenderholt, and K. M. Langner. cclib: A library for package-independent computational chemistry algorithms, 2008. doi:10.1002/jcc.20823.

[42] M. Jamróz. Vibrational energy distribution analysis veda 4, 2004.

[43] Thomas Kluyver, Benjamin Ragan-Kelley, Fernando Pérez, Brian Granger, Matthias Bussonnier, Jonathan Frederic, Kyle Kelley, Jessica Hamrick, Jason Grout, Sylvain Corlay, Paul Ivanov, Damon Lee, Safia Abdalla, and Carol Willing. Jupyter notebooks – a publishing format for reproducible computational workflows. *Positioning and Power in Academic Publishing: Players, Agents and Agendas*, pages 87–90, 2016. doi:10.3233/978-1-61499-649-1-87.

[44] Dassault Systèmes BIOVIA. Discovery studio visualizer, 2021. URL: https://www.3ds.com/products-services/biovia/products/biovia-discovery-studio/.

[45] Mario S Valdés-Tresanco, Mario E Valdés-Tresanco, Pedro A Valiente, and Ernesto Moreno. Amdock: a versatile graphical tool for assisting molecular docking with autodock vina and autodock4. *Biology direct*, 15:1–12, 2020.

[46] Warren L. DeLano. Pymol: A molecular graphics system, 2002. Version 2.5.2, Schrödinger, LLC. URL: http://www.pymol.org.

[47] Roman A. Laskowski and Mark B. Swindells. Ligplot+: Multiple ligand–protein interaction diagrams for drug discovery. *Journal of Chemical Information and Modeling*, 51(10):2778–2786, 2011.

[48] Antoine Daina, Olivier Michielin, and Vincent Zoete. Swissadme: a free web tool to evaluate pharmacokinetics, drug-likeness and medicinal chemistry friendliness of small molecules. *Scientific reports*, 7(1):42717, 2017.

[49] Priyanka Banerjee, Emanuel Kemmler, Mathias Dunkel, and Robert Preissner. Protox 3.0: a webserver for the prediction of toxicity of chemicals. *Nucleic Acids Research*, page gkae303, 2024.

[50] Timothy J Snape, Alison M Astles, and Janice Davies. Understanding the chemical basis of drug stability and degradation. *Pharmaceutical journal*, 285(7622):416–417, 2010.

[51] Konstantin N Kudin and Gustavo E Scuseria. Linear-scaling density-functional theory with gaussian orbitals and periodic boundary conditions: Efficient evaluation of energy and forces via the fast multipole method. *Physical Review B*, 61(24):16440, 2000.

[52] Jamshed Haneef, Mohd Amir, Nadeem Ahmed Sheikh, and Renu Chadha. Mitigating drug stability challenges through cocrystallization. *AAPS PharmSciTech*, 24(2):62, 2023.

[53] Noureddine Issaoui, Houcine Ghalla, S Muthu, HT Flakus, and Brahim Oujia. Molecular structure, vibrational spectra, aim, homo–lumo, nbo, uv, first order hyperpolarizability, analysis of 3-thiophenecarboxylic acid monomer and dimer by hartree–fock and density functional theory. *Spectrochimica acta part a: molecular and biomolecular spectroscopy*, 136:1227–1242, 2015.

[54] Eric J Lien, Zong-Ru Guo, Ren-Li Li, and Ching-Tang Su. Use of dipole moment as a parameter in drug–receptor interaction and quantitative structure–activity relationship studies. *Journal of pharmaceutical sciences*, 71(6):641–655, 1982.

[55] Florbela Pereira and João Aires-de Sousa. Machine learning for the prediction of molecular dipole moments obtained by density functional theory. *Journal of cheminformatics*, 10:1–11, 2018.

[56] E Barim and Feride Akman. Synthesis, characterization and spectroscopic investigation of n-(2-acetylbenzofuran-3-yl) acrylamide monomer: Molecular structure, homo–lumo study, td-dft and mep analysis. *Journal of Molecular Structure*, 1195:506–513, 2019.

[57] Rashmi Mishra, Bhawani Datt Joshi, Anubha Srivastava, Poonam Tandon, and Sudha Jain. Quantum chemical and experimental studies on the structure and vibrational spectra of an alkaloid–corlumine. *Spectrochimica Acta Part A: Molecular and Biomolecular Spectroscopy*, 118:470–480, 2014.

[58] P.W. Atkins, J. De Paula, and J. Keeler. *Atkins' Physical Chemistry*. Oxford University Press, 2018. URL: https://books.google.com.np/books?id=3QpDDwAAQBAJ.

[59] Muna T Tayyem and Mansour H Almatarneh. A dft computational study of the antioxidant activities exhibited by3-aryl-4-hydroxycoumarin derivatives. *J Chem Appl Biochem*, 3:119, 2016.

[60] R Fouad and Omima MI Adly. Novel cu2+ and zn2+ nanocomplexes drug based on hydrazone

ligand bearings chromone and triazine moieties: Structural, spectral, dft, molecular docking and cytotoxic studies. *Journal of Molecular Structure*, 1225:129158, 2021.

[61] R Parthasarathi, Venkatraman Subramanian, Debesh R Roy, and PK Chattaraj. Electrophilicity index as a possible descriptor of biological activity. *Bioorganic & medicinal chemistry*, 12(21):5533–5543, 2004.

[62] Robert G Parr, László v Szentpály, and Shubin Liu. Electrophilicity index. *Journal of the American Chemical Society*, 121(9):1922–1924, 1999.

[63] Bhargab Borah and Th Gomti Devi. Characterization of zn (l-proline) 2 complex using spectroscopic techniques and dft analysis. *Journal of Molecular structure*, 1210:128022, 2020.

[64] S Gunasekaran, R Arun Balaji, S Kumeresan, G Anand, and S Srinivasan. Experimental and theoretical investigations of spectroscopic properties of n-acetyl-5-methoxytryptamine. *Can. J. Anal. Sci. Spectrosc*, 53(4):149–162, 2008.

[65] Zeynep Demircioğlu, Çiğdem Albayrak Kaştaş, and Orhan Büyükgüngör. Theoretical analysis (nbo, npa, mulliken population method) and molecular orbital studies (hardness, chemical potential, electrophilicity and fukui function analysis) of (e)-2-((4-hydroxy-2-methylphenylimino) methyl)-3-methoxyphenol. *Journal of Molecular structure*, 1091:183–195, 2015.

[66] Mohammed S Taghour, Hazem Elkady, Wagdy M Eldehna, Nehal El-Deeb, Ahmed M Kenawy, Eslam B Elkaeed, Bshra A Alsfouk, Mohamed S Alesawy, Dalal Z Husein, Ahmed M Metwaly, et al. Design, synthesis, anti-proliferative evaluation, docking, and md simulations studies of new thiazolidine-2, 4-diones targeting vegfr-2 and apoptosis pathway. *PLoS One*, 17(9):e0272362, 2022.

[67] M. Khadka, M. Sah, R. Chaudhary, and S. K. Sahani. Spectroscopic, quantum chemical, and topological calculations of the phenylephrine molecule using density functional theory. *Scientific Reports*, 15:81633, 2025. doi:10.1038/s41598-024-81633-2.

[68] Kirk E Hevener, Wei Zhao, David M Ball, Kerim Babaoglu, Jianjun Qi, Stephen W White, and Richard E Lee. Validation of molecular docking programs for virtual screening against dihydropteroate synthase. *Journal of chemical information and modeling*, 49(2):444–460, 2009.

[69] G.N. Ramachandran, C. Ramakrishnan, and V. Sasisekharan. Stereochemistry of polypeptide chain configurations. *Journal of Molecular Biology*, 7(1):95–99, 1963. doi:https://doi.org/10.1016/S0022-2836(63)80023-6.

[70] Murat Cihan Sorkun, Abhishek Khetan, and Süleyman Er. Aqsoldb, a curated reference set of aqueous solubility and 2d descriptors for a diverse set of compounds. *Scientific data*, 6(1):143, 2019.

[71] P Fonteh, A Elkhadir, B Omondi, I Guzei, J Darkwa, and Debra Meyer. Impedance technology reveals correlations between cytotoxicity and lipophilicity of mono and bimetallic phosphine complexes. *Biometals*, 28:653–667, 2015.

[72] Christopher A Lipinski, Franco Lombardo, Beryl W Dominy, and Paul J Feeney. Experimental and computational approaches to estimate solubility and permeability in drug discovery and development settings. *Advanced drug delivery reviews*, 64:4–17, 2012.

[73] William M Pardridge. The blood-brain barrier: bottleneck in brain drug development. *NeuroRx*, 2(1):3–14, 2005.

[74] Sukanth Kumar Enmozhi, Kavitha Raja, Irudhayasamy Sebastine, and Jerrine Joseph. Andrographolide as a potential inhibitor of sars-cov-2 main protease: an in silico approach. *Journal of biomolecular structure and dynamics*, 39(9):3092–3098, 2021.

[75] Christophe Herkenne, Ingo Alberti, Aarti Naik, Yogeshvar N Kalia, François-Xavier Mathy, Véronique Préat, and Richard H Guy. In vivo methods for the assessment of topical drug bioavailability. *Pharmaceutical research*, 25:87–103, 2008.